

Thermal vibration and melting from a local perspective

Edward A. Stern, Pēteris Līviņš, and Zhe Zhang

Department of Physics, FM-15, University of Washington, Seattle, Washington 98195

(Received 18 September 1990)

X-ray-absorption fine-structure (XAFS) measurements of lead from 10 K through and above the melting transition at 600 K have been carried out. A cumulant expansion analysis provides data on the first four moments of the radial distribution of the first shell, which are used to construct a consistent temperature-dependent radial distribution function for the solid. The distribution is one given by a simple one-dimensional anharmonic oscillator. The results also demonstrate that XAFS, a local probe, can clearly distinguish between the liquid and solid state. In the liquid, the apparent coordination number is decreased by the fraction of the time the atom is diffusing. An improved method for determining the background at low k is discussed that gives a reliable determination of the background much closer to the threshold than allowed by standard methods.

I. INTRODUCTION

The melting phase transformation from a solid to a liquid in three dimensions is well understood thermodynamically. However, thermodynamics is not a complete description of the phenomenon. Many physical details need to be filled in. For example, the structure differences between the two phases have to be ascertained; the microscopic mechanisms that initiate the transformation and the kinetics of the transformation need to be elucidated. The usual way to describe the structural difference between the solid and liquid phases is in terms of long-range order. The ideal solid has long-range order which produces sharp Bragg diffraction peaks while the liquid has no long-range order and thus no sharp diffraction peaks.

Even more striking than loss of long-range order is the difference in mechanical rigidity between a solid and a liquid. The solid is much more resistant to shear stress than is the liquid. Under normal conditions the shape of a solid is not significantly modified under weak shear stresses while a liquid has no resistance to shear stress and consequently its shape is determined by its container. There are some liquids that are quite viscous, and solids near their melting point show creep under shear, so that the difference in the rigidity to shear is not absolute. However, there is a discontinuity in shear resistance at the melting point.

The Stokes-Einstein relation relates the viscosity inversely to the self-diffusion coefficient, indicating that the microscopic mechanism that leads to loss of shear resistance is diffusion of atoms. At the melting point the self-diffusion rate of metals typically increases by a factor of 10^5 , producing the discontinuity in the mechanical properties. This discontinuity in diffusion is the most striking change that occurs in a local perspective of melting.

Because melting is a first-order phase transition, long-range fluctuations are not a significant factor and the loss of long-range order occurs by atomic mechanisms which are short ranged. For that reason, observing the melting

phenomenon from a local atomic perspective may give more insight into the mechanism of the melting process than can be obtained from diffraction studies. This paper presents the results of an experimental investigation of melting of pure Pb from a local viewpoint using the x-ray-absorption fine-structure technique (XAFS).^{1,2}

There are several techniques that can measure atomic correlations from a local perspective. These are XAFS, Mössbauer effect, diffuse coherent scattering, and incoherent neutron scattering. Diffuse coherent scattering³ in monatomic systems measures the instantaneous pair-correlation function, which gives the probability of finding an atom a distance from another atom. XAFS also measures this same correlation function, and has the advantage of distinguishing the center and neighboring atoms, while also having more sensitivity for dilute atoms. However, its range is limited to about 4–5 Å while diffuse coherent scattering can probe much further. By use of contrast variation or anomalous scattering methods, diffuse coherent scattering can also distinguish atoms, but with much greater effort and in some limited cases. The Mössbauer effect measures,⁴ for time periods of the order of its lifetime, the Fourier transform of the self-correlation function of the Mössbauer atom at the wave number $k = E_\gamma / \hbar c$ of the Mössbauer γ ray of energy E_γ (here \hbar is Planck's constant divided by 2π and c is the velocity of light). Incoherent neutron scattering also measures a similar quantity⁵ and with the flexibility of varying both k and time intervals, though it cannot measure as long a time interval as the Mössbauer effect and it cannot focus on a particular atom.

The increase in diffusion rate at melting is so great that the recoilless Mössbauer signal usually disappears in the liquid. This loss of recoilless fraction is taken as the signature of the occurrence of melting. In this paper we show that XAFS also has a distinctive signature of melting by investigating pure Pb through its melting point. Because of its lower sensitivity to diffusion than the Mössbauer effect, XAFS detects a signal in the liquid, and is therefore able to elucidate some of the local prop-

erties in the liquid state. In addition, XAFS measurements in the solid determine the anharmonic contribution to the thermal vibrations. By correctly accounting for this anharmonicity, it is possible to determine the thermal expansion, and various moments of the distribution function between an atom and its first neighbors. The difficulty introduced by anharmonicity, first pointed out by Eisenberger and Brown,⁶ is overcome by the cumulant expansion^{1,7,8} approach employed here.

Section II describes the experimental details of an XAFS study of thermal disorder in lead. Section III presents the experimental results and discusses the analysis. Section IV contains a discussion and interpretation of the experimental results and a summary is presented in Sec. V.

II. EXPERIMENTAL DETAILS

The Pb sample was prepared from 99.999%-pure Pb shot which was evaporated in a 10^{-6} -Torr vacuum onto a 0.0025-cm-thick Al foil to the desired thickness. In order to prevent oxidation of the Pb and to act as a container after it liquifies, an aluminum coating about 2 μm thick was evaporated on the exposed surfaces of the Pb film, including its edges. It was important to cover the edges because, previously, when the edges were not covered, the whole sample oxidized after it melted.

The XAFS measurements were made at beamline X11A at the National Synchrotron Light Source (NSLS). The energy resolution of the x rays was optimized by closing down the slits in front of the I_0 ion chamber till no further increase in resolution was attained, as ascertained by observing the sharpness of near-edge features in the Pb L_3 edge. The energy resolution was then limited by either the resolution of the Si(111) monochromator crystals or the lifetime broadening at the L_3 edge of Pb, whichever is greater. In any case, any further narrowing of the slits would not have improved the energy resolution of our data but would have decreased the detected x-ray intensity.

The XAFS above room temperature was measured by transmission on the pure Pb sample with a thickness x and absorption coefficient μ corresponding to a $\Delta\mu x = 0.87$ at the L_3 edge to minimize thickness effects.⁹ The x-ray harmonics were minimized by detuning the two crystal monochromator to about 70–80% of the maximum value. This amount of detuning has been shown to effectively eliminate harmonics at X11A with this monochromator at this energy.

The sample was heated in a furnace with kapton windows which was evacuated by a mechanical pump for thermal isolation. The vacuum was not sufficient to protect against oxidation. This protection was afforded by the aluminum coating. The furnace could cover the temperature range from room temperature to above the bulk melting temperature of Pb of 600 K. The temperature of the sample was monitored by two chrome-alumel thermocouples placed so that they monitored the temperature gradient across the sample holder in addition to the average temperature.

Previous attempts to measure the XAFS of the sample

as it melted were unsuccessful because the integrity of the sample was destroyed as it coagulated into numerous droplets of liquid. This time the Al coating and the Pb sample both maintained their integrity sufficiently for successful measurements on the liquid phase. However, the melted sample sagged under gravity within its aluminum coating. This sagging caused the $\Delta\mu x$ of the region exposed to the x rays to change from 0.87 to 0.18. The liquid Pb did not oxidize during the measurement. This was determined in two ways. The XAFS showed no signal from oxygen neighbors and after the sample was resolidified, it returned to the same XAFS signal as before, though with the smaller $\Delta\mu x$ step.

Another possible explanation for the decreases in $\Delta\mu x$ and XAFS signal after melting is x-ray leakage around the sample. If the sample lost its integrity after melting, then part of the x-ray beam could pass through the sample without passing through Pb. This leakage has the effect of decreasing both $\Delta\mu x$ and the XAFS signal spuriously.⁹ It is therefore important to eliminate this possibility.

The following checks were made to discount this possibility. The x-ray beam was moved vertically on the sample and the transmitted intensity decreased by a factor of 2 as the beam moved to the bottom of the sample, as expected by sagging. The beam was also moved to another sample and the same XAFS were found as for the first sample. It would be unlikely that both samples would have similar leakage effects. Finally, the most definitive measurement was to measure the XAFS on the sample after it resolidified. The $\Delta\mu x$ in the solid state remained reduced but the XAFS increased to the value of the solid. The change in XAFS was reversible even though the change in $\Delta\mu x$ was not. This is consistent only with sagging and not leakage.

The measurements below room temperature were also done by transmission. The samples for these measurements were again produced by vacuum evaporation, but on a 0.0025-cm-thick kapton substrate. The samples were sealed in a copper cell under a helium atmosphere which maintained thermal contact between the cell and the samples. The cell was attached to the cold finger of an Air Products' displax refrigerator whose temperature was monitored by a Cu-Au:Fe thermocouple. Both the temperature at the center of the cell and the gradient along the cell were monitored.

III. EXPERIMENTAL RESULTS AND ANALYSIS

The XAFS of the sample was measured at various temperatures from 10 K up to above the melting point. Far from the melting point T_m , the temperature steps were large, reducing to 4 K near T_m . Figure 1(a) shows x-ray-absorption data for the L_3 edge of solid Pb at 30 K, at room temperature, and at 598 K, showing the usual attenuation caused by the increasing amplitude of thermal vibrations. Figure 1(b) shows the abrupt drop in XAFS amplitude that occurs from 598 to 602 K as the sample melts at 600 K.

The analysis of the data requires subtraction of the background to isolate the oscillatory XAFS signal. An

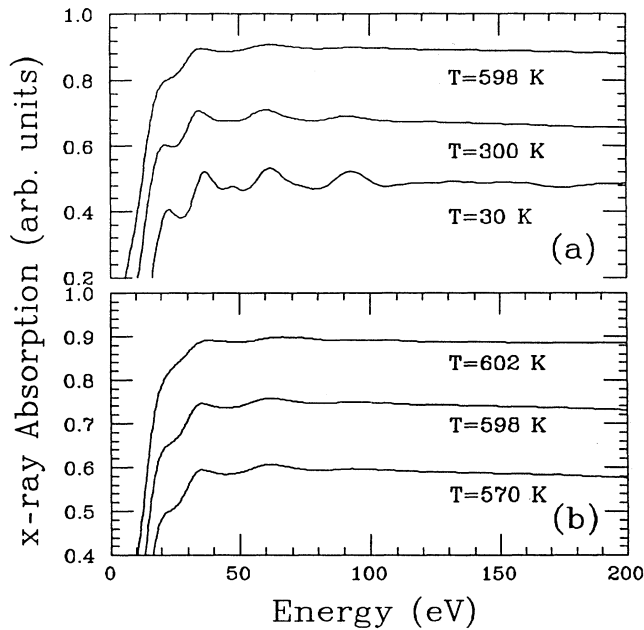


FIG. 1. X-ray-absorption spectra for Pb illustrating the gradual change (a) from low to high temperature in the solid and (b) the abrupt change at the solid to liquid transition.

inspection of Fig. 1 makes it clear that the standard method of background subtraction will severely limit the range over which the significant XAFS signal can be isolated for the high-temperature scans. Because of the attenuation caused by the large vibrational disorder present at temperatures near T_m , the signal is significant only near the edge. In addition, this attenuation is compounded by a deep minimum in the XAFS scattering amplitude occurring at $k \approx 6 \text{ \AA}^{-1}$, effectively forcing an upper limit there for analysis at temperatures above room temperature. Here k is defined in Eq. (1).

The standard method of background subtraction assumes smooth, more or less monotonic, variation of the background. This is valid in this case beyond 55 eV ($k = 3.8 \text{ \AA}^{-1}$) past the edge as illustrated in Fig. 2 for Pb at 460 K, and indicated by the downward arrow. However, as the edge is approached, the background starts rounding into the edge. The edge itself is quite broad, of the order of 20 eV. This width is significantly larger than the L_3 -edge lifetime broadening of 10 eV. Also, there is an obvious XAFS contribution near the top of the edge at about 20 eV. Since near T_m most of the significant signal is nearer the edge than can be isolated by the standard background analysis, we are forced to search for a new method. To accomplish this, we use two new constraints to determine the background in the edge region, which permits reliable background subtraction, in this case, down into the edge to the limit indicated (12 eV) by the upward arrow in Fig. 2.

First we note that by definition the background must pass through those points that correspond to zeros in the XAFS signal. We find the energies where such zero

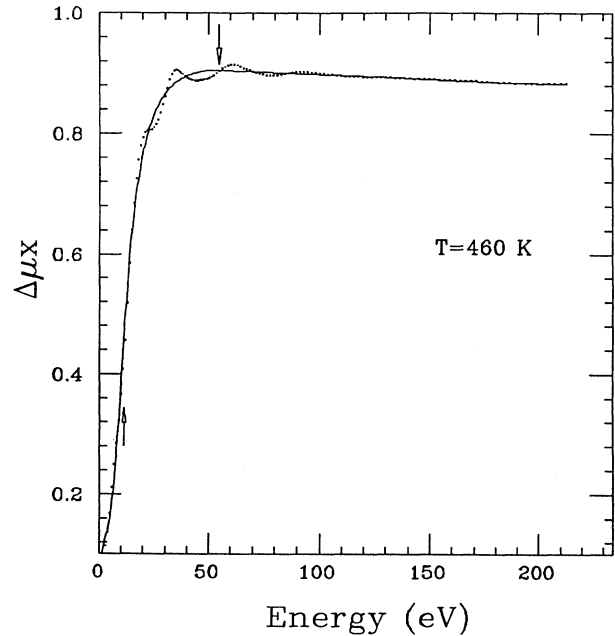


FIG. 2. The background (solid line) determined for Pb data (dotted line) at $T=460 \text{ K}$. The downward arrow denotes the limit for reliable background determination when using a simple smooth monotonic fit. The upward arrow shows the extended range with the method proposed here.

crossings occur by carefully subtracting the total absorption signals from one another at various temperatures, thus obtaining difference spectra (Fig. 3). If the phase difference between XAFS of different temperatures is negligible, then increasing temperatures simply attenuate the amplitude of the XAFS signal and the differences will have zero crossings at the same energies where the background must pass through the absorption data itself. It is at low wave number that an assumption of negligible

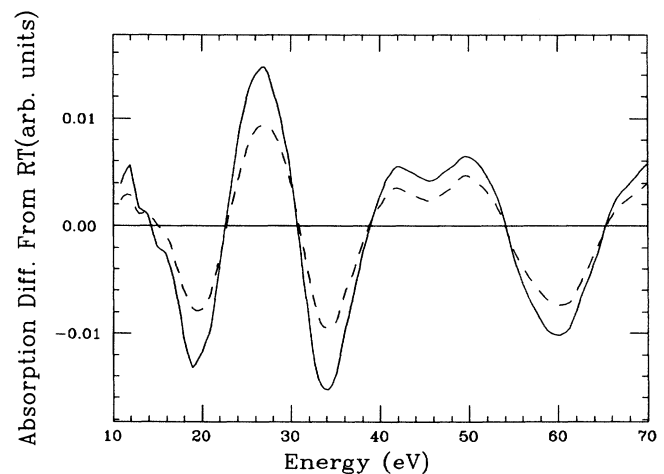


FIG. 3. Difference spectra of 570-K data (solid line) and 460-K (dashed line) data, both taken with respect to 300-K data.

phase difference can be valid. The cumulant expansion of the XAFS phase [Eq. (6)] shows that for small enough k the phase difference between the XAFS signal of different temperatures varies linearly with wave number. The linear coefficient is usually small enough that at low wave numbers the assumption of negligible phase difference is very good. Knowing energy points through which the background must pass through the data in the low- k limit provides constraints on a smooth background fit through the data. This fit is smoothly extended at higher k where standard approaches are adequate.

The other constraint recognizes that the oscillator sum rule¹⁰ implies that the total area of the XAFS signal integrates to zero. The sum rule requires the same total absorption independent of the temperature. Increasing temperature causes disorder which decreases the XAFS signal, and in the hypothetical case of very high temperature with the solid maintaining its structure, only the background remains. Thus, the background itself satisfies the sum rule, and the XAFS signal must integrate to zero. With a reliable background in the high- and low- k regions, this additional constraint helps fix the background determination at the extreme low- k limit where the data crossing on the sharply changing edge is more difficult to obtain accurately.

Our analysis will be directed at obtaining relative phase and amplitude information between XAFS of different temperatures. Clearly, constructing a background where one forces the different temperature XAFS at low k to be in phase will cancel any sensitivity to relative phase information in the constrained region. However, when the phase differences are small there, the relative amplitude information will be insensitive to such errors, and thus accurate throughout the constrained region. In this report we determine data crossings that allow a reliable XAFS amplitude determination as low as $\approx 1.7 \text{ \AA}^{-1}$. The constrained background fit reaches as high as 3.2 \AA^{-1} , thus usable relative phase information starts above this value. With this extension of the XAFS data to lower wave number, we obtain values of the first four moments of the pair distribution function about the Pb host atoms all the way to and above the melting point.

It should be mentioned, since the XAFS signal is a small percentage of the total absorption signal, that obtaining the difference spectra requires careful alignment and scaling of the different temperature XAFS spectra. This is facilitated when the measuring instrumentation, x-ray beam, and calibration are reasonably stable. If complete data are taken with an eye for such conditions, we feel it is possible to go one step further in advancing the background determination. One can take the difference spectra of one temperature with all other temperatures above and below the temperature in question. The energy corresponding to a particular zero crossing of the difference spectra, when plotted as a function of temperature difference, can be interpolated or extrapolated to zero temperature difference, giving the correct energy for the data crossing at the temperature being analyzed. In this way the XAFS spectrum at each temperature would have its own set of energies through which the background must intersect the data. Thus, the loss of relative

phase information in the constrained region is avoided.

One might question whether the XAFS so close to the edge can be analyzed assuming single scattering, as is done for data further past the edge. In fact, this question motivated the distinction between the x-ray-absorption near-edge structure (XANES) and the extended x-ray-absorption fine structure (EXAFS) because it was argued that multiple scattering is dominant in the XANES while single scattering is dominant in the EXAFS.¹¹ However, subsequent experiment¹² and theoretical investigations¹³ have shown that type-2 multiple scattering paths are not as dominant in the XANES region as previously thought, where type 2 denotes ones for which the alignment of scattering atoms deviates significantly from colinearity. In particular, when one is considering the first shell,¹⁴ as we are doing here, there is rigorously *no* multiple scattering contribution whatsoever throughout the full XAFS range, including the XANES region because multiple scattering contributions add to the signal only beyond the first shell. In Pb, for example, the first multiple scattering contribution is about half the first neighbor distance past the first shell, i.e., about 1.75 \AA beyond the first shell. It should be emphasized that we are not assuming that multiple scattering is negligible in the near-edge region, only that it does not contribute to the isolated first shell XAFS, which is rigorous. Thus, there is no need to distinguish between XANES and EXAFS, and one can utilize all of the XAFS range to obtain structural information, as we are doing here.

The XAFS $\chi(k)$, as a function of wave number k for several temperatures are shown in Fig. 4. The values of k in \AA^{-1} are determined from

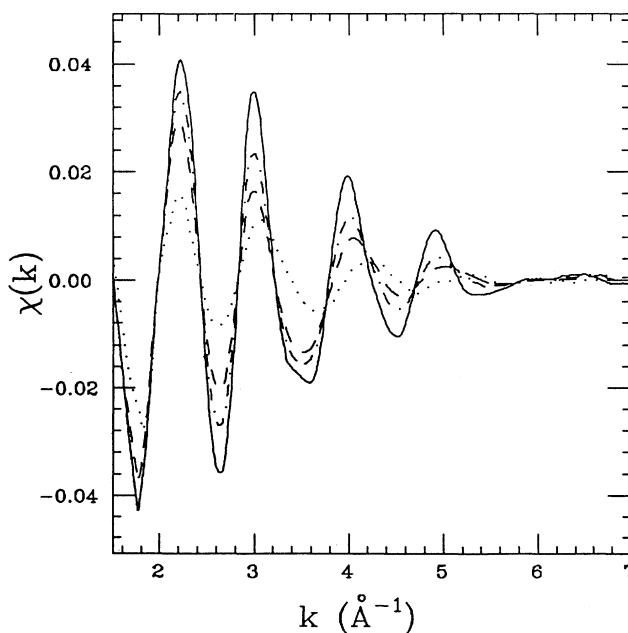


FIG. 4. $\chi(k)$ for Pb in the solid state at $T=300 \text{ K}$ (solid line), 460 K (dot-dashed line), 598 K (dashed line), and in the liquid state at 602 K (dotted line).

$$k = [0.263(E - E_0)]^{1/2}, \quad (1)$$

where E is the photon energy in eV and E_0 is set below the energy of the midpoint of the Fermi edge step by the free-electron Fermi energy using a density of electrons of four electrons per Pb atoms. The $\chi(k)$ is evaluated by

$$\chi(k) = \left[\frac{\mu(k) - \mu_0(k)}{\Delta\mu_0} \right], \quad (2)$$

where $\mu(k)$ is the measured absorption, $\mu_0(k)$ is the background determined as described above, and $\Delta\mu_0$ is the L_3 -edge step. Fourier transforms of $k^2\chi(k)$ of Fig. 4 are shown in Fig. 5, evaluated over the range $1.7 \text{ \AA}^{-1} < k < 6.5 \text{ \AA}^{-1}$. As can be noted from Fig. 5, the major contribution to the XAFS is from the first shell. The first shell is isolated at each temperature by the window functions shown in Fig. 5 and back Fourier transformed into k space. The ln ratios of amplitude and phase difference between various temperatures are calculated. The cumulant expansion of such ln ratios and phase differences can be made near $k=0$, giving for the amplitude ratio,

$$\ln \frac{A_1}{A_2} = \Delta a - 2k^2\Delta\sigma^2 + \frac{2}{3}\Delta b k^4, \quad (3)$$

where A_1 and A_2 are the XAFS amplitude at the two temperatures T_1 and T_2 , respectively. Data at T_2 will be

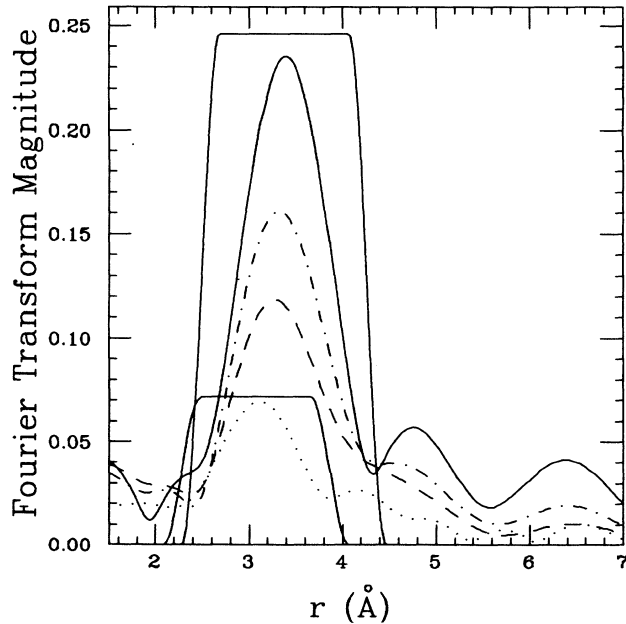


FIG. 5. Fourier transforms of $k^2\chi(k)$ and first-shell filtering windows for Pb in the solid state at $T=300$ K (solid line), 460 K (dot-dashed line), 598 K (dashed line), and the liquid state at 602 K (dotted line). The window shifted to the left corresponds to the liquid state only.

referred to as the standard. Here Δa is the change in N/R^2 between the two temperatures, where R is the average distance to the first shell and N is the number of nearest-neighbor atoms; $\Delta\sigma^2$ is the change in the mean-squared deviation from R between the two temperatures; and Δb is the difference of the fourth cumulant between the two temperatures. The fourth cumulant is equal to

$$b = \langle (r-R)^4 \rangle - 3\sigma^4, \quad (4)$$

where $\langle (r-R)^4 \rangle$ is the fourth moment of the disorder of the nearest-neighbor atoms about their average value of R . The mean-squared deviation is given by

$$\sigma^2 = \langle (r-R)^2 \rangle. \quad (5)$$

The cumulant expansion of the phase difference is of the form

$$\Delta\phi = 2k\Delta R - \frac{4}{3}\Delta c k^3, \quad (6)$$

where ΔR is the change in the average distance and Δc is the change in the third cumulant between the two temperatures. The third cumulant

$$c = \langle (r-R)^3 \rangle \quad (7)$$

is equal to the third moment of the disorder about R . It should be noted that the above moments are defined about R , the average radial distance between the absorbing atom, and the backscattering atom at the temperature T , which is different from the distance at $T=0$.

Both the ln ratio and the phase difference of the Pb data above room temperature are fit by their respective cumulant expansions [Eqs. (3) and (6), respectively]. Above room temperature we are limited in the data range to below 6 \AA^{-1} , beyond which the minimum in the scattering amplitude makes an accurate analysis difficult. Here, we use the room-temperature data as the standard, fitting over the range $2 \text{ \AA}^{-1} < k < 5 \text{ \AA}^{-1}$ for the amplitude ratio and $3.4 \text{ \AA}^{-1} < k < 5.25 \text{ \AA}^{-1}$ for the phase difference. One advantage the ln-ratio method provides is a cancellation of the broadening effects due to the finite-energy resolution of the spectrometer. Since the low-temperature data were obtained with a different energy resolution, it was not possible to use a single standard throughout the whole low- and high-temperature range. One could use the room-temperature data obtained with the low-temperature group as the standard for the low-temperature data, and thus reference all results with respect to room temperature. However, this has the disadvantage of limiting the analysis range below 6 \AA^{-1} even for the low-temperature spectra, where useful data extends beyond this limit. Thus we use the 10-K data as the standard for the data below room temperature, and fit, omitting the region $5.5 \text{ \AA}^{-1} < k < 7 \text{ \AA}^{-1}$ where the noise is large because of the minimum in the signal, from $2 \text{ \AA}^{-1} < k < 9.5 \text{ \AA}^{-1}$ for the amplitude ratio and $7.5 \text{ \AA}^{-1} < k < 9.5 \text{ \AA}^{-1}$ for the phase difference. For the phase below room temperature, we omit fitting the low- k region because there the very small phase differences are obscured by the filtering leakage, again caused by the noise of the backscattering amplitude minimum. The two data sets, below and above room temperature, are

TABLE I. Lowest-order temperature coefficients of the first four cumulants for Pb, obtained for temperatures up to the melting point.

$\Delta R/T$ ($10^{-5} \text{ \AA}/\text{K}$)	σ^2/T ($10^{-5} \text{ \AA}^2/\text{K}$)	c/T^2 ($10^{-8} \text{ \AA}^3/\text{K}^2$)	b/T^3 ($10^{-12} \text{ \AA}^4/\text{K}^3$)
8.0 ± 3.4	9.9 ± 1.2	1.9 ± 0.2	6.6 ± 3.3

then linked by making the room-temperature results match, effectively referencing all the results to the 10-K data. We then fit the temperature dependence of the cumulants from above the Einstein temperature ($\approx 66 \text{ K}$) to just before melting, the range where classical behavior for the vibrations is expected. As discussed in Sec. IV, these fits use a T , T^2 , or T^3 dependence, obtaining the values of $\Delta R/T$, σ^2/T , c/T^2 , and b/T^3 , listed in Table I.

A test of the new background subtraction method can be made by the low-temperature data. In that case the \ln ratio should have a small contribution from Δb since thermal anharmonicities should be weak. Plots of \ln ratio versus k^2 should be a smooth curve with little k^4 contribution, even up to high- k values where the standard background subtraction applies. Figure 6(a) shows such plots for $T=100$ and 200 K , using the 10-K data as the standard. In the intermediate range centered at $k=6 \text{ \AA}^{-1}$ the data become unreliable because of the minimum in the backscattering amplitude. As can be noted, the linear low- k behavior matches smoothly with the non-linear high- k behavior. However, at elevated temperatures, anharmonicity will produce significant Δb terms

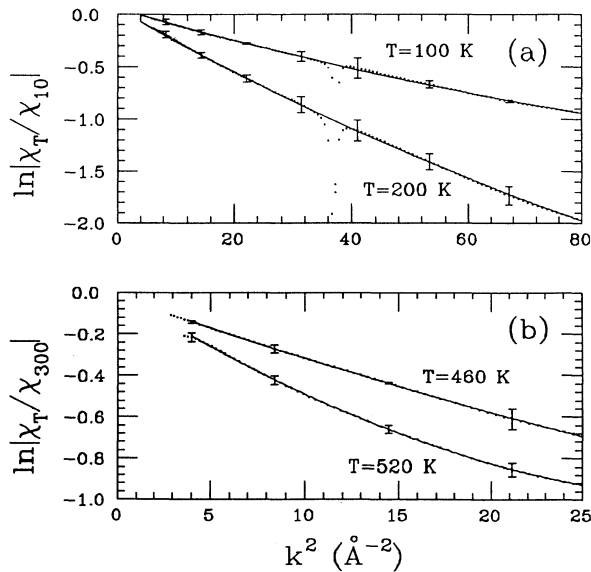


FIG. 6. Typical data (dots) and cumulant fits (solid) to the \ln ratio of the first-shell amplitudes for Pb at various temperatures, illustrating the onset of anharmonicity with temperature. The error bars represent the spacing of independent data points.

even below the backscattering minimum and the non-linear curve of Fig. 6(b) results as the temperature increases from $T=460 \text{ K}$ to $T=520 \text{ K}$, where the room-temperature data are used as the standard. Similarly, Fig. 7 shows the cumulant fits to the phase for various temperatures.

The error bars of Figs. 6 and 7 are generated using the rms deviation from the average value of the log ratio or phase difference. The averages are obtained from slightly different background removals using the variations in data-crossing energies obtained from different difference spectra and also using different data scans at any one temperature. Furthermore, we include a $\pm 0.1 \text{ \AA}$ variation of the filtering window width and also a $\pm 0.3 \text{ \AA}^{-1}$ shift of the fitting range. The spacing of the error bars indicates the spacing of independent data points after Fourier filtering. The spacing δk between independent points is given by¹⁵

$$\delta k = \frac{\pi}{2\delta R}, \quad (8)$$

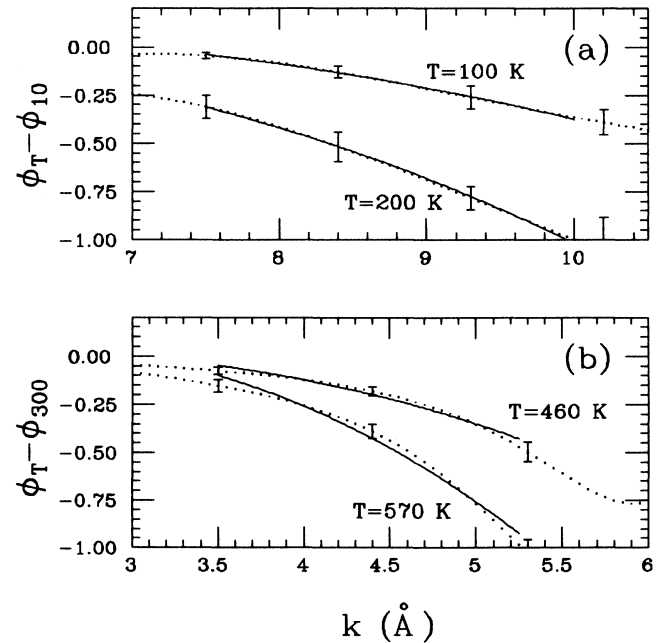


FIG. 7. Typical phase difference (dots) and fits (solid) to the first shell for low- and high-temperature ranges. The error bars represent the spacing of independent data points.

where δR is the r -space filter-window width. In our case δR is 1.8 Å; thus δk is approximately 0.87 \AA^{-1} .

IV. RESULTS AND DISCUSSION

Plots of $\Delta\sigma^2$ and ΔR versus T/T_m are presented in Fig. 8, of Δc versus $(T/T_m)^2$ and Δb versus $(T/T_m)^3$ in Fig. 9, and of $\exp\Delta a$ versus T/T_m in Fig. 10. The changes in ΔR , $\Delta\sigma^2$, and Δb obtained at low temperatures should fit smoothly with the high-temperature values, showing, as they do, the consistency between the standard background subtraction and improved method

$$\begin{aligned} \langle (z - \langle z \rangle) \rangle &= \frac{\int_{-\infty}^{\infty} (z - \langle z \rangle)^n \exp\left[\frac{-V(z)}{k_B T}\right] dz}{\int_{-\infty}^{\infty} \exp\left[\frac{-V(z)}{k_B T}\right] dz} \\ &\approx \frac{\int_{-\infty}^{\infty} (z - \langle z \rangle)^n \exp\left[\frac{-kz^2}{2k_B T}\right] \left[\sum_{n=0}^3 \frac{1}{n!} \left(\frac{gz^3 + fz^4}{k_B T}\right)^n \right] dz}{(2\pi k_B T/k)^{1/2} \left[1 + \frac{3(k_B T)}{k^2} [f + 5g^2/(2k)] \right]} \end{aligned} \quad (10)$$

to the lowest orders in T , are

$$\langle z \rangle = \frac{3gk_B T}{k^2} \left[1 + \frac{k_B T}{k^2} (32f + 45g^2/k) \right], \quad (11)$$

$$\langle (z - \langle z \rangle)^2 \rangle = \frac{k_B T}{k} \left[1 + \frac{3k_B T}{k^2} (4f + 12g^2/k) \right], \quad (12)$$

one here.

We can model the temperature dependence of the anharmonic effects by considering a one-dimensional potential V expanded about its minimum at R_0 ,

$$V(z) = \frac{1}{2}kz^2 - gz^3 - fz^4. \quad (9)$$

Here z represents the displacement about R_0 . Within the classical limit and the assumption that the anharmonicity can be treated as a small perturbation, the temperature dependence of the moments about the mean $\langle z \rangle$, as determined by evaluating the thermal average

$$\langle (z - \langle z \rangle)^3 \rangle = \frac{6g(k_B T)^2}{k^3} \left[1 + \frac{6k_B T}{k^2} (9f + 24g^2/k) \right], \quad (13)$$

$$\langle (z - \langle z \rangle)^4 \rangle = \frac{3(k_B T)^2}{k^2} \left[1 + \frac{4k_B T}{k^2} (8f + 27g^2/k) \right]. \quad (14)$$

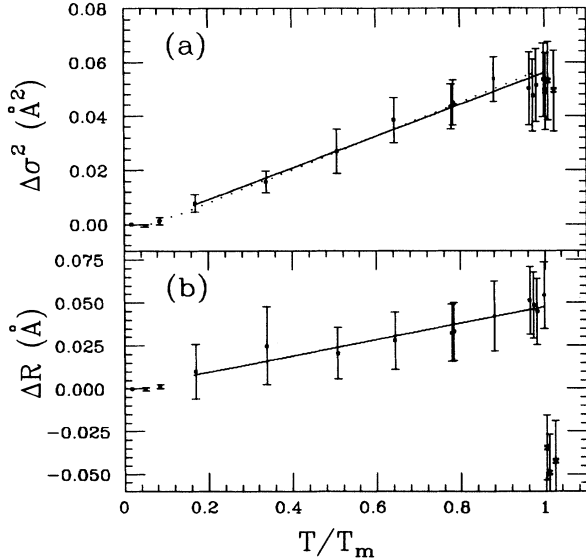


FIG. 8. Linear fits to (a) $\Delta\sigma^2$ and (b) ΔR vs temperature. Also shown (dots) is a fit to σ^2 modeled with an Einstein oscillator. The points denoted by crosses correspond to the liquid.

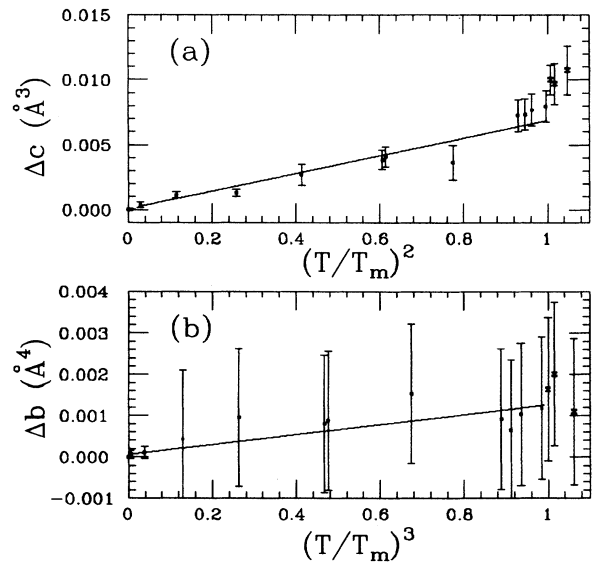


FIG. 9. Linear fits to (a) Δc and (b) Δb plotted as a function of T^2 and T^3 , respectively. The points denoted by crosses correspond to the liquid.

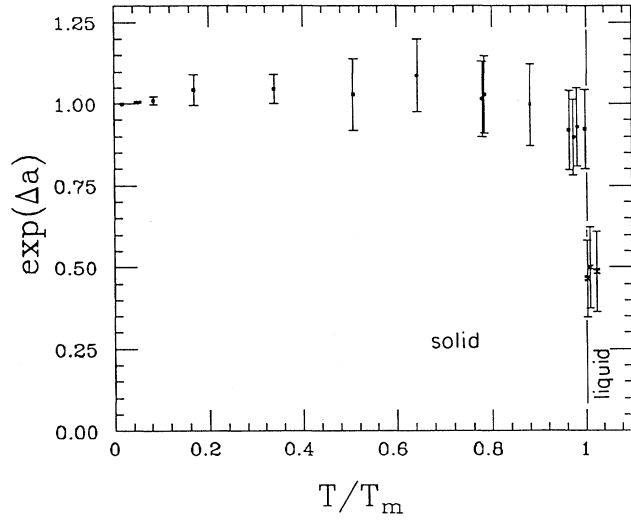


FIG. 10. Plot of $\exp(\Delta a)$ vs temperature, illustrating the apparent loss of coordination number at the melting temperature. The points denoted by crosses correspond to the liquid.

The truncation of the series in Eq. (10) serves as a convergence cutoff while including enough terms to accurately obtain the second lowest-order expressions for the moments. The respective cumulants obtained from Eqs. (11)–(14) to lowest order in T are

$$\Delta R = \frac{3gk_B T}{k^2}, \quad (15)$$

$$\sigma^2 = \frac{k_B T}{k}, \quad (16)$$

$$c = \frac{6g(k_B T)^2}{k^3}, \quad (17)$$

and noting Eq. (4),

$$b = 12 \frac{(k_B T)^3}{k^4} (2f + 9g^2/k). \quad (18)$$

To lowest order, σ^2 and ΔR are expected to be linear with T while c and b are expected to vary as T^2 and T^3 , respectively, consistent with the experimental results for the solid. Also, Δa is expected to be zero for the solid, again in agreement with experiment.

Note from Table I that $b \ll 3\sigma^4$. This means that $\langle (r-R)^4 \rangle \approx 3\sigma^4$, from Eq. (4). This result is what is obtained for a Gaussian distribution where all cumulants are zero except for the second one. Since, to lowest order, σ^2 is linear in T , the fourth moment varies as T^2 . Also shown in Fig. 8 is the temperature dependence of σ^2 for an Einstein oscillator.¹ The fit to the experimental data gives $\Theta_E = 66$ K.

The results obtained by the data analysis can be summarized by a distribution function $p(r)$ of the relative distance between a Pb atom and its first-shell nearest neighbors, which we write as

$$p(r) = \frac{[1 + \gamma(r-R_0)^3 + \xi(r-R_0)^4]}{(2\pi\sigma^2)^{1/2}(1 + 3\xi\sigma^4)} \times \exp\left[\frac{-(r-R_0)^2}{2\sigma^2}\right], \quad (19)$$

where

$$\gamma = \frac{c}{6\sigma^6} \approx \frac{g}{k_B T} \quad (20)$$

and

$$\xi = \frac{1}{8\sigma^8} \left[\frac{b}{3} - \frac{c^2}{\sigma^2} \right] \approx \frac{f}{k_B T}. \quad (21)$$

The above $p(r)$ approximates the classical distribution function of the one-dimensional anharmonic oscillator, as suggested by the Boltzmann factor of Eq. (10). Here k , g , and f are expressed through the cumulants σ , c , and b by using their lowest-order relations, Eqs. (16)–(18), respectively.

To lowest order, the first moment of the above-modified Gaussian function is written¹

$$\langle R - R_0 \rangle = \frac{c}{2\sigma^2}. \quad (22)$$

The relation of Eq. (22) implies that the linear thermal expansion coefficient α , is given by

$$\alpha = \frac{c}{2\sigma^2 T R_0}. \quad (23)$$

It should be noted that since the modified Gaussian function is a direct consequence of the anharmonic function of Eq. (9), the relation in Eq. (23) follows directly from the anharmonic one-dimensional oscillator.

Substituting the values of c and σ^2 determined by XAFS (Table I) and the value (at 25°C) (Ref. 16) of $R_0 = 3.49$ Å gives a predicted result of $\alpha = (2.8 \pm 0.5) \times 10^{-5} \text{ K}^{-1}$. The value as measured directly here by XAFS is $(2.3 \pm 1.0) \times 10^{-5} \text{ K}^{-1}$. The average value determined by microscopic measurements¹⁷ is $(3 \pm 0.2) \times 10^{-5} \text{ K}^{-1}$. It is impressive that the simple function of Eq. (19) can predict the thermal expansion. It appears that the distribution of the relative distance between Pb atoms can be described by a simple one-dimensional anharmonic oscillator. The linear expansion is caused by the cubic term in the anharmonic expansion which also produces the third moment of the distribution function. As can be noted for XAFS, the thermal expansion is more accurately determined by the third moment than by a direct determination. Thus, the thermal expansion can be determined from the third moment when it is too small to be determined directly. This result has been used to estimate the thermal expansion of the bond length of surface atoms.¹⁸

From the value of σ^2 in Table I and Eq. (16), we find that the force constant $k = 0.87 \pm 0.1 \text{ eV \AA}^{-2}$. The ratio of third to first moments from the XAFS data is $(2.4 \pm 0.4)\sigma^2$. Within our uncertainties, this is consistent with the value of $2\sigma^2$ predicted from the lowest-order terms of the one-dimensional anharmonic oscillator.

However, since our direct measurement of the first moment in XAFS is not as accurate as the macroscopic measurement, we obtain a more accurate ratio by using the macroscopic measurement for the thermal expansion. The resulting ratio is $(1.8 \pm 0.3)\sigma^2$. The third moment is more reliable than the first, and from Eq. (20) we estimate the cubic anharmonic term $g = 0.28 \pm 0.09 \text{ eV}/\text{Å}^3$. Also, from Eq. (21) the quartic term $f = -0.15 \pm 0.17 \text{ eV}/\text{Å}^4$. These results are summarized in Table II.

We pause here to point out that the cumulant expansion coefficients are more correctly moments about the average of a function $P(r)$, where¹

$$P(r) = \frac{R^2}{r^2} p(r) e^{[-2(r-R)]/\lambda}, \quad (24)$$

with the one-dimensional distribution $p(r)$ satisfying

$$\int p(r) dr = 1. \quad (25)$$

Here λ is the mean free path of the photoelectron. The distribution $p(r)$ may be related to the three-dimensional radial density function $\rho(r)$ by

$$p(r) = \frac{4\pi r^2 \langle \rho(\mathbf{r}) \rangle \Omega}{N} \quad (26)$$

and thus

$$P(r) = \frac{4\pi R^2}{N} e^{[-2(r-R)]/\lambda} \rho(r), \quad (27)$$

where $\langle \rangle \Omega$ denotes an angular average, $\rho(r) = \langle \rho(\mathbf{r}) \rangle \Omega$, and N is the coordination number of the shell. For that shell,

$$\int \rho(\mathbf{r}) d^3r = N. \quad (28)$$

Also, the corresponding pair distribution function $g(\mathbf{r})$ is simply related to the radial density function through the particle number density ρ_0 by

$$\rho(\mathbf{r}) = \rho_0 g(\mathbf{r}). \quad (29)$$

The differences between moments of $p(r)$, $\rho(r)$, and $P(r)$ are negligible when σ^2/R^2 and σ/λ are small.

In the liquid the assumption of anharmonicity as a small perturbation is no longer valid and one does not expect the simple $p(r)$ of Eq. (19) to apply. The most striking change that occurs on melting is the change in Δa . In the case of a solid,

$$\exp(\Delta a) = \frac{1 + \Delta N/N}{(1 + \Delta R/R)^2}. \quad (30)$$

Since the change in R is small, Eq. (30) implies that the large change in Δa is due to a large change in N . However, the change in density of only a few percent on melting

is too small to be consistent with the large change in N .

This drop in the coordination number is just apparent and actually reflects the fact that the Fourier transform does not include data down to zero wave number, and thus misses the broad structureless contribution due to the large disorder component caused by diffusion. After melting, the diffusion rate in lead¹⁹ increases about five orders of magnitude to a value of $D \approx 2.5 \times 10^{-5} \text{ cm}^2 \text{ sec}^{-1}$. We can estimate the hopping rate of Pb atoms in the liquid from the formula²⁰

$$D \approx (n/3)l^2, \quad (31)$$

where n is the number of successful hops per second and l is an interatomic distance, which is 3.5 Å for Pb. The estimate for n is 6×10^{10} per second. Since the Einstein temperature corresponding to the thermal vibration of the Pb atom corresponds to a frequency of 1.4×10^{12} Hz, there occurs about one hop per 23 oscillations. During a successful hop where a Pb atom moves a distance l , its environment will be too disordered to produce any XAFS signal. The lowest k value that we analyze is 1.5 Å^{-1} . Since the XAFS signal strength is attenuated by the factor $\exp(-2k^2\sigma^2)$, an estimate of the largest mean-square disorder σ^2 that can still produce an XAFS signal is $2 \times 1.5^2 \times \sigma^2 = 1$, or $\sigma = 0.5 \text{ Å}$. In the midst of the hopping of 3.5 Å, the disorder will be greater than this value of σ and no XAFS will be produced.

The XAFS signal for the liquid is decreased by η , the fraction of the time that an atom spends accomplishing a successful hop. This allows a determination of the average number of vibrations the lead atom makes before diffusing again. Denoting the average time the Pb atom requires to complete a single successful hop as τ , then

$$\eta = n\tau. \quad (32)$$

The experiment indicates that $\eta \approx 0.5$, giving a value of $\tau = 8.2 \times 10^{-12}$, which corresponds to 11 periods of vibration to complete a single successful hop.

We also note that from Figs. 8 and 9 that ΔR and the third moment c change abruptly at melting. This also partly reflects the effect of the finite low- k cutoff. Another way to describe this is that the XAFS can only observe the "sharp" portion of $p(r)$ in the liquid. On melting, c increases roughly 30% and ΔR shows roughly a 0.09-Å drop. Since the density of Pb decreases on melting, ΔR should increase, but not necessarily the first moment of the sharp part of $p(r)$.

To understand these results, the XAFS changes on melting are compared with diffuse x-ray scattering results. Figure 11 plots the $\rho(r)$ of the solid at 600 K given by Eq. (19) and $\rho(r)$ of liquid Pb given by diffuse x-ray scattering.²¹ The XAFS results are for only the first coordination shell of Pb atoms. In drawing the $\rho(r)$ of the solid we assumed that the second and third shells have similar values²² of ratio to the first shell as σ^2 values in Cu metal, which also has an fcc structure. This assumption is only approximately true, but the figure does illustrate the essential difference between the $\rho(r)$ of the solid and liquid. The liquid shows much larger values of $\rho(r)$ between shells than in the solid. These intershell values are caused by the diffusion in the liquid.

TABLE II. The harmonic force constant k with the cubic g and quartic f anharmonic constants obtained for Pb.

k (eV/Å ²)	g (eV/Å ³)	f (eV/Å ⁴)
0.87 ± 0.1	0.28 ± 0.09	-0.15 ± 0.17

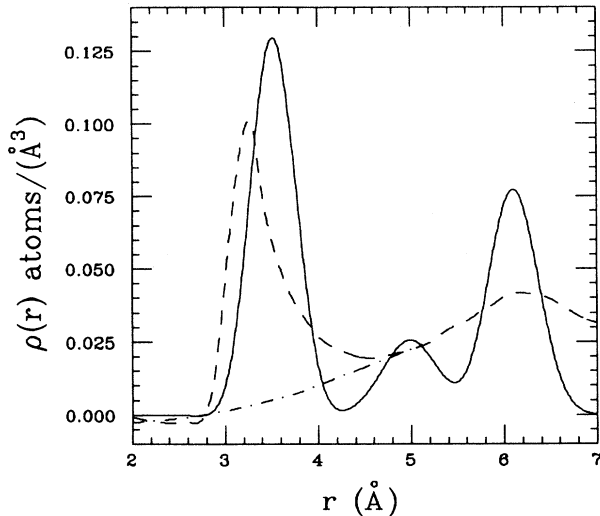


FIG. 11. The radial density function $\rho(r)$ for liquid Pb just above the melting point (solid line), obtained from diffuse x-ray scattering. For comparison, the $\rho(r)$ for the solid just below melting constructed with Eq. (19), using the results of the cumulant expansion data (Table I). The dot-dashed line is an estimate of the smooth structureless background for the first shell contributed by diffusion in the liquid state.

We can attempt to isolate the sharp part of $\rho(r)$ for a liquid by drawing a smooth and structureless reasonable background for the first shell of the radial density function obtained from the diffuse x-ray scattering, as shown in Fig. 11. Subtracting this smooth background, the resulting sharp portion of $\rho(r)$ gives a first moment of 3.43 Å. This matches the abrupt 0.09-Å drop observed in Fig. 8(b), since just before melting ΔR is ≈ 3.52 Å. Furthermore, the area is 30% smaller, in reasonable qualitative agreement with the 50% drop discussed above. The higher moments are in poorer agreement, but this should be expected since they are more sensitive to the arbitrarily drawn structureless background. The sharp portion of the diffuse scattering $\rho(r)$ has all the features detected by XAFS: a smaller area leading to the decrease in a , and a larger asymmetry leading to the larger third moment. Thus the XAFS and diffuse scattering results are consistent with one another when one remembers that the XAFS analysis of cumulants applies only to the sharp portion of $\rho(r)$.

V. SUMMARY

The results on Pb illustrate clearly that XAFS can distinguish between the liquid and solid state. Since XAFS is a local probe, it detects the difference locally. This shows in two main ways, a decrease in a , the apparent coordination number, and an increase in the third mo-

ment of $\rho(r)$ indicating an increase in asymmetry. Interestingly, for liquid Pb, σ^2 does not change significantly on melting. The decrease in apparent coordination number is caused by diffusion, leading to an estimate of the time it takes for a Pb atom to complete a successful hop. This change on melting is pertinent to the interpretation of premelting phenomena around impurities as observed²³ by XAFS. It was observed for Hg impurities in Pb that above 400 K, well below the bulk melting temperature, the apparent coordination number starts decreasing significantly while σ^2 saturates. This behavior is consistent with a microscopic liquid region forming around the impurities as the measurements here indicate. The connection to local premelting was made previously by analysis of the temperature dependence of $\rho(r)$ for liquid Pb as determined by diffuse x-ray scattering. The measurements presented here confirm that analysis. It should be pointed out that because of its greater sensitivity and capability to focus on a particular atom, XAFS can determine the local premelting about dilute impurities, a result that cannot be detected by diffuse scattering.

The measurements in the solid show that XAFS can detect the anharmonic contributions to the thermal relative motion of the Pb atoms to its nearest neighbors. It should be noted that XAFS measures the relative vibration motion in contrast to the Bragg diffraction Debye-Waller factor which measures the vibration motion about a lattice site. The thermal expansion can be explained by the cubic term of the $\rho(r)$ in Eq. (19). The combination of the cubic term and the increasing values of σ^2 with temperature cause the thermal expansion as given in Eq. (23). As far as we know, this is the most accurate determination of $\rho(r)$ of the first shell in a solid as a function of temperature up to melting. It is striking that the data are consistent with the $\rho(r)$ that is precisely what one expects from a simple one-dimensional anharmonic oscillator whose anharmonicity is a small perturbation. Our measurements define the anharmonic potential to the fourth order in the displacements. The first four moments were determined to the accuracy attained because of the introduction of a new method of background subtraction in the absorption spectra of XAFS which allowed the determination of the signal in regions within the edge which were traditionally thought inaccessible.

ACKNOWLEDGMENTS

One of us (E. A. S.) is indebted to Professor John Cahn for many informative conversations. We also appreciate help provided by other members of our research group, who include Dr. S. Lin, M. Qian, Y. Zhang, M. Newville, and B. Ravel. This research was funded by U. S. Department of Energy (DOE) Contract No. DE-FG-84ER45163. We also thank the NSLS, supported under DOE Contract No. DE-AC0276CH00016.

- ¹E. A. Stern and S. M. Heald, in *Handbook on Synchrotron Radiation*, edited by E. E. Koch (North-Holland, New York, 1983), Vol. 1, p. 955.
- ²P. A. Lee, P.H. Citrin, P. Eisenberger, and B. M. Kincaid, *Rev. Mod. Phys.* **53**, 76 (1981).
- ³See, for instance, Y. Waseda, *Structure of Non-Crystalline Materials* (McGraw-Hill, New York, 1980).
- ⁴K. S. Singwi and A. Sjolander, *Phys. Rev.* **120**, 1093 (1960).
- ⁵L. Van Hove, *Phys. Rev.* **95**, 1374 (1954).
- ⁶P. Eisenberger and G. S. Brown, *Solid State Commun.* **29**, 481 (1979).
- ⁷G. Bunker, *Nucl. Instrum. Methods* **207**, 437 (1982).
- ⁸E. D. Crozier, R. Ingalls, and J. J. Rehr, in *EXAFS*, edited by R. Prins and D. Kroningsberger (Wiley, New York, 1988).
- ⁹E. A. Stern and K. Kim, *Phys. Rev. B* **23**, 3781 (1981).
- ¹⁰See, for instance, B. K. Agarwal, *X-ray Spectroscopy* (Springer-Verlag, Berlin, 1979), p. 374.
- ¹¹E. A. Stern, *Phys. Rev. B* **10**, 3027 (1974).
- ¹²G. Bunker and E. A. Stern, *Phys. Rev. Lett.* **52**, 1990 (1984).
- ¹³D. D. Vvedensky and J. B. Pendry, *Phys. Rev. Lett.* **54**, 2725 (1985); G. Bunker and E. A. Stern, *ibid.* **54**, 2726 (1985).
- ¹⁴P. A. Lee and J. B. Pendry, *Phys. Rev. B* **11**, 2795 (1975).
- ¹⁵See, for instance, *Proceedings of the Fifth International Conference on X-Ray Absorption Fine Structure*, edited by Mustre de Leon *et al.* (North-Holland, Amsterdam, 1989), p. 710.
- ¹⁶W. B. Pearson, *Handbook of Lattice Spacings and Structures of Metals* (Pergamon, Oxford, 1958), p. 126.
- ¹⁷*American Institute of Physics Handbook*, edited by D. E. Gray (McGraw-Hill, New York, 1963), pp. 4–66.
- ¹⁸Wenzel *et al.*, *Phys. Rev. Lett.* **64**, 1765 (1990).
- ¹⁹J. R. Wilson, *Metall. Rev.* **10**, 381 (1965).
- ²⁰See, for instance, F. Reif, *Fundamentals of Statistical and Thermal Physics* (McGraw-Hill, New York, 1965), p. 485.
- ²¹See Y. Waseda, *Structure of Non-Crystalline Materials* (Ref. 3), pp. 274 and 275.
- ²²E. A. Stern, B. A. Bunker, and S. M. Heald, *Phys. Rev. B* **21**, 5521 (1980).
- ²³E. A. Stern and K. Zhang, *Phys. Rev. Lett.* **60**, 1872 (1988).